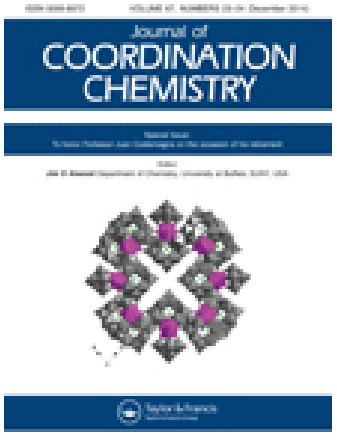

Journal of Coordination Chemistry
Publication details, including instructions for authors and subscription information:
http://www.tandfonline.com/loi/gcoo20

A TiO_2@{Mo_{368}} composite: synthesis, characterization, and application in dye-sensitized solar cells

Yanhua Wang[a], Jiansheng Li[a], Xiaojing Sang[a], Weilin Chen[a], Zhongmin Su[a] & Enbo Wang[a]

[a] Key Laboratory of Polyoxometalate Science of Ministry of Education, Department of Chemistry, Northeast Normal University, Changchun, Jilin, PR China

Accepted author version posted online: 13 Oct 2014.Published online: 03 Nov 2014.

Journal of Coordination Chemistry, 2014
Vol. 67, Nos. 23–24, 3873–3883, http://dx.doi.org/10.1080/00958972.2014.976211

A TiO_2@{Mo_{368}} composite: synthesis, characterization, and application in dye-sensitized solar cells

YANHUA WANG, JIANSHENG LI, XIAOJING SANG, WEILIN CHEN*, ZHONGMIN SU and ENBO WANG*

Key Laboratory of Polyoxometalate Science of Ministry of Education, Department of Chemistry, Northeast Normal University, Changchun, Jilin, PR China

(*Received 28 May 2014; accepted 29 September 2014*)

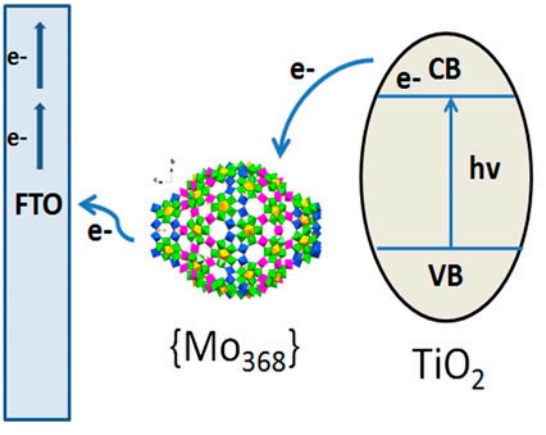

The high-nuclear cluster compound $Na_{48}[H_xMo_{368}O_{1032}(H_2O)_{240}(SO_4)_{48}]\cdot ca.1000H_2O$ (denoted as {Mo_{368}}) represents the known nanoscale hedgehog-type cluster anion with the diameter of approximately 6 nm. Herein, a TiO_2@{Mo_{368}} composite was prepared through a sol–gel process for the first time. SEM, XPS, and UV–vis spectra were employed to characterize their chemical composition and structures. Meanwhile, the as-obtained composite was further mixed with P25 (Degussa P25 titania photocatalyst) then applied as the photoanodes of dye-sensitized solar cells (DSSCs); the results showed that DSSCs with the P25-TiO_2@{Mo_{368}}-based photoanodes exhibited better performance than that with pure P25-based photoanodes, which was due to less carrier recombination and longer electron lifetime in the former DSSCs by the results from analysis of dark current measurement, electrochemical impedance spectroscopy, and open-circuit voltage decay curve.

Keywords: Polyoxometalates; High-nuclear cluster; Dark current; Titanium dioxide; Dye-sensitized solar cells

*Corresponding authors. Email: chenwl@nenu.edu.cn (W. Chen); wangeb889@nenu.edu.cn (E. Wang)

1. Introduction

Dye-sensitized solar cells (DSSCs) have attracted widespread concern of both scientific research and industrial fields since their discovery in 1991 due to their low cost, facial operation, and stable performance [1]. DSSCs are composed of four parts, a semiconductor photoanode, sensitizers, electrolyte with a redox couple, and a counter electrode [2]. The preparation craft of the photoanodes is crucial to the overall power conversion efficiency of DSSCs [3]. A variety of different semiconductors have been used to prepare the photoanodes [4]. The most common material is TiO_2 which exhibits very high stability [5]. However, several kinds of carrier recombinations still existed in the TiO_2-based photoanodes, and the dominant one is the recombination of injected conduction band electrons with the oxidized dyes and oxidized species in the electrolyte [6]. Therefore, reducing recombination is expected to further improve the overall photoelectric conversion efficiency of DSSCs. According to the literature, modification of TiO_2 with certain doping agents is an effective way to suppress the recombination and enhance electron transport [7]. Graphene and carbon nanotubes have been applied to modify the photoanodes of DSSCs [8].

Polyoxometalates (POMs) are a unique class of molecular metal–oxygen clusters, which have received wide attention in catalysis, medicine, and materials science field owing to their versatile structures and compositions [9]. POMs have excellent redox properties and are capable of accepting or releasing multiple electrons reversibly without changing their structures [10]. Therefore, POMs could be applied as an electron mediator to reduce the carrier recombination on the surface of TiO_2 or ZnO for enhancing their photocatalytic or photovoltaic conversion capability [11]. The commonly used one is the classic Keggin or Dawson structure, and there is little research about other types of POMs [12]. The high nucleation of POMs is one research hotspot of POMs chemistry [13]. The high-nuclear metal–oxygen clusters not only have unique structures, but also nanometer size [14]. Hence, they show broad application prospects in materials science [15]. Recently, we reported a spherical keplerate $\{W_{72}V_{30}\}$ acting as the electron acceptor in a photovoltaic system which is a promising alternative electron acceptor to the traditional electron acceptor fullerene (C60) [16]. High-nuclear molybdenum clusters represent another kind of typical compound. Prof. A. Müller has conducted the most thorough research for this system [17]. Thereinto, $\{Mo_{368}\}$ reached the highest high-nuclear metal–oxygen cluster system, which represents an unusual giant hedgehog-shaped molybdenum oxide-based nanocluster with the size of approximately 6 nm and containing 368 metal atoms [18]. Furthermore, there are two kinds of molybdenum ions with different valences existing in this compound. These features relating to the unusual structure and mixed valence could be expected to make $\{Mo_{368}\}$ transport electrons effectively. Thus, we prepared a $TiO_2@\{Mo_{368}\}$ composite to confirm whether the nanoscale hetero blue $\{Mo_{368}\}$ could enhance the photoelectric conversion efficiency of TiO_2-based photovoltaic system as an electron mediator. In this paper, the sol–gel technique was employed to prepare $TiO_2@\{Mo_{368}\}$ composite, which was further mixed with P25, then applied as the photoanode of DSSCs. The results show that the introduction of $TiO_2@\{Mo_{368}\}$ composite could effectively improve the short-circuit current and open-circuit voltage of DSSCs through suppressing the dark current and increasing the electron lifetime.

2. Experimental

2.1. *General methods and materials*

All chemicals were commercially purchased and used without purification. {Mo_{368}} was prepared according to the literature [19] and characterized by FTIR spectra (figure S1, see online supplemental material at http://dx.doi.org/10.1080/00958972.2014.976211) and cyclic voltammetry. FTIR spectrum was recorded from 400–4000 cm^{-1} on an Agilent Technologies FTIR spectrometer. UV–vis absorption spectra were obtained using a 752 PC UV–vis spectrometer. The diffuse reflectivity spectra were collected on a SHIMADZU UV–vis Spectrophotometer UV-2600 in reflectance mode, measured from 200 to 800 nm using barium sulfate ($BaSO_4$) as a standard with 100% reflectance. Thermal stability of {Mo_{368}} was determined by TG analysis on a Perkin-Elmer TGA7 instrument in flowing N_2 with a heating rate of 10 °C min^{-1}. The electrochemical experiments were recorded on a CHI 601D electrochemical workstation at room temperature using glassy carbon electrode as the working electrode, a Pt wire as the counter electrode, and Ag/AgCl as the reference electrode. 0.5 M Na_2SO_4/H_2SO_4 with pH 1.5 was used as the supporting electrolyte. XPS was performed on F-doped SnO_2 glass using an ESCALAB-MKII photoelectronic spectrometer with a Mg $K\alpha$ (1253.6 eV) achromatic X-ray source. The morphology and structure of TiO_2@{Mo_{368}} composite as well as the morphology and chemical composition of the composite of P25-TiO_2@{Mo_{368}} were characterized with a scanning electron microscope (SEM; XL-30 ESEM FEG, Micro FEI Philips) at an accelerating voltage of 20 kV. All the photoelectrochemical experiments were performed using a potentiostat (CS 350, Wuhan CorrTest Instrument Co. Ltd, China) at room temperature equipped with a Xenon lamp as the light source.

2.2. *Preparation of TiO_2@{Mo_{368}} composite*

TiO_2@{Mo_{368}} composite was prepared with the method similar to that reported in the literature [20]. Five milliliters of titanium isopropoxide was dissolved in 3 mL n-butyl alcohol to give a solution (A), and 0.05 g {Mo_{368}} was dissolved in distilled water to form a dark blue solution (B). Then the solution B was added dropwise into solution A with stirring. The mixture was heated at 45 °C and 80 °C for 3 h, successively. The resulting hydrogel was placed in a 45 °C vacuum oven for 12 h and then maintained at 80 °C for 3 h. After washing five times by distilled water, it was dried at 80 °C for 3 h. Finally, TiO_2@{Mo_{368}} composite was obtained.

2.3. *Fabrication of DSSCs*

Firstly, P25 powder was sintered at 400 °C for 30 min. Then the TiO_2 paste was prepared according to a similar method in the literature by mixing TiO_2@{Mo_{368}} composite and the calcined P25 with a mass fraction of 0.5%. The photoanodes were prepared by coating one layer of paste on the FTO glass plates which had been ultrasonic cleaned in detergent solution and absolute ethanol for 30 min, respectively, by screen-printing followed by drying for 5 min at 120 °C [21]. This screen-printing procedure was repeated four times to control the thickness of the working electrode. After drying in air, the P25-TiO_2@{Mo_{368}} composite films were calcined in air at 325 °C for 30 min. Subsequently, the resulting sintered films were post-treated in 40 mM $TiCl_4$ solution for 30 min at 70 °C and calcined in air at 325 °C for 30 min again.

The obtained TiO_2 electrodes were immersed in a 0.2 mM N719 absolute ethanol solution for 24 h at room temperature to complete the sensitizer uptake. The excess unanchored dyes were rinsed off with absolute ethanol and dried with N_2. Then the dye-covered TiO_2 electrodes were covered with platinum mirror as counter electrodes. An electrolyte solution composed of 0.1 M LiI, 0.05 M I_2, 0.6 M 1,2-dimethyl-3-propylimidazolium iodide, and 0.5 M 4-tert-butylpyridine in 3-methoxypropionitrile was introduced between the electrodes by the capillary action.

3. Results and discussion

3.1. *Photoelectrochemical property of {Mo_{368}}*

The electrochemical properties of {Mo_{368}} were investigated by cyclic voltammetric method in the pH 1.5 Na_2SO_4/H_2SO_4 electrolyte solution at a scan rate of 100 mVs^{-1}, as shown in figure 1(a). There are two cathodic peaks located at −0.18 V and −0.62 V, which correspond to the redox processes of Mo^{VI} and Mo^{V} centers in the polyoxoanion framework and are accompanied by their anodic peaks at −0.44 V and −0.072 V, respectively. Because the lowest unoccupied molecular orbitals (LUMO) of POMs are formally the combination of d orbitals centered on the metal atoms [22], the LUMO of {Mo_{368}} could be estimated by its onset reduction potential that is positioned at 0.32 V *versus* normal hydrogen electrode (NHE). Figure 1(b) shows the UV–vis absorption spectrum of {Mo_{368}} aqueous solution. It can be seen that {Mo_{368}} exhibits wide absorption covering UV, near-infrared to the visible region. The UV light absorption was related to the charge transfer from oxygen to metal while the absorption from near-infrared to the visible region was attributed to Mo(V) d–d transitions and Mo(V)–Mo(VI) intervalence charge transfer (IVCT) transitions in the {Mo_{368}} framework [23]. The inset of figure 1(b) shows the schematic energy levels of TiO_2 and {Mo_{368}}, which indicated that {Mo_{368}} possessed a lower LUMO level than that of the conduction band of TiO_2. Hence, {Mo_{368}} is expected to act as an electron acceptor for suppressing the carrier recombination on the surface of TiO_2.

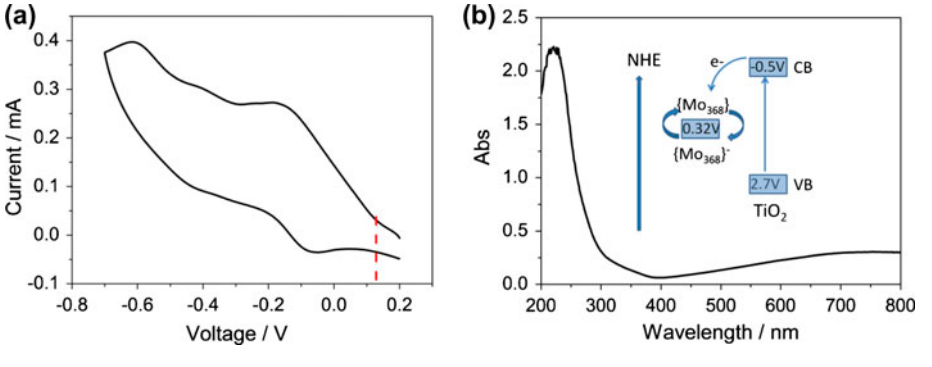

Figure 1. (a) The cyclic voltammogram of {Mo_{368}} in Na_2SO_4/H_2SO_4 electrolyte solution with pH 1.5; (b) UV–vis absorption spectrum of {Mo_{368}} aqueous solution; the inset is the schematic energy level of TiO_2 and {Mo_{368}}.

3.2. *Characterization of TiO_2@{Mo_{368}} and the composite film of P25-TiO_2@{Mo_{368}}*

The solid diffuse reflection spectrum was employed to characterize the UV–vis absorption of the as-obtained TiO_2@{Mo_{368}} powder (shown in figure 2), and for comparison the UV–vis absorption of P25 and {Mo_{368}} were both studied. P25 exhibits its characteristic absorption in only the UV region because of its wide bandgap. {Mo_{368}} shows broad absorption covering the entire UV, visible, and near-infrared regions, which is consistent with its absorption spectra in aqueous solution. The enhanced absorption in the visible and near-infrared scale could result from light scattering between solid particles. Finally, the prepared TiO_2@{Mo_{368}} composite displays both stronger UV and visible-to-near infrared absorption, which confirmed the successful composition of TiO_2 and {Mo_{368}}.

The XPS spectrum was employed to characterize the oxidation state of Ti and Mo. Figure 3(a) shows the XPS spectra for Ti which exhibits two peaks located at about 464.2 eV in the energy region of $Ti2p_{1/2}$ and around 458.4 eV in the energy region of $Ti2p_{3/2}$, which correspond to the Ti^{IV} oxidation state [24]. The binding energy at about

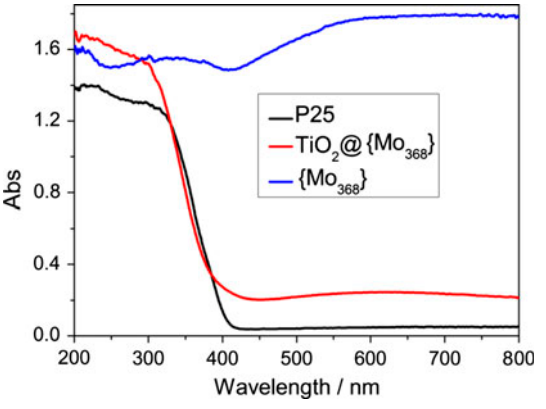

Figure 2. Solid diffuse reflection spectrum of P25 (dark line); TiO_2@{Mo_{368}} (red line); and {Mo_{368}} powder (blue line) (see http://dx.doi.org/10.1080/00958972.2014.976211 for color version).

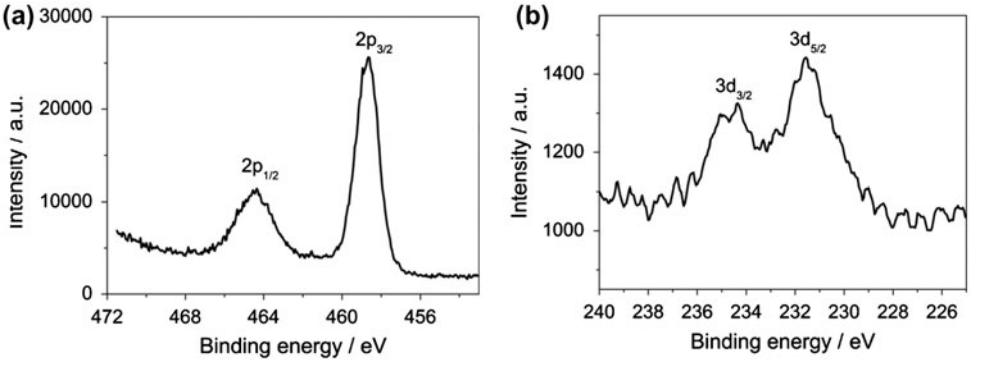

Figure 3. The XPS spectrum for Ti_{2p} (a) and Mo_{3d} (b) of the TiO_2@{Mo_{368}} composite.

231.6 eV and 234.4 eV are attributed to $Mo3d_{5/2}$ and $Mo3d_{3/2}$, respectively [25], which indicated that $\{Mo_{368}\}$ was incorporated into TiO_2.

Figure 4 shows the SEM images of $TiO_2@\{Mo_{368}\}$ compared with pure $\{Mo_{368}\}$. As can be seen, the pure $\{Mo_{368}\}$ shows the irregular block structure with micron-grade size, which is due to the large aggregation of $\{Mo_{368}\}$. Compared with $\{Mo_{368}\}$, the $TiO_2@\{Mo_{368}\}$ composite enters into the dispersed nanoparticles with size of around 100 nm, which laid a foundation for introducing this composite into the photoanodes of DSSCs. However, some particle aggregates still exist in the composite. Further, the thermal stability of $\{Mo_{368}\}$ was investigated by thermogravimetric analysis. Figure S2 shows its TG curve which displays a two-step weight loss from 30 to 600 °C. The first step corresponds to loss of water and the second one is related to the structure collapse of the polyoxoanion. This result indicated that the structure of $\{Mo_{368}\}$ remained after sintering at 325 °C. Figure 5 shows the SEM image and EDX diagram of the composite film of P25-$TiO_2@\{Mo_{368}\}$.

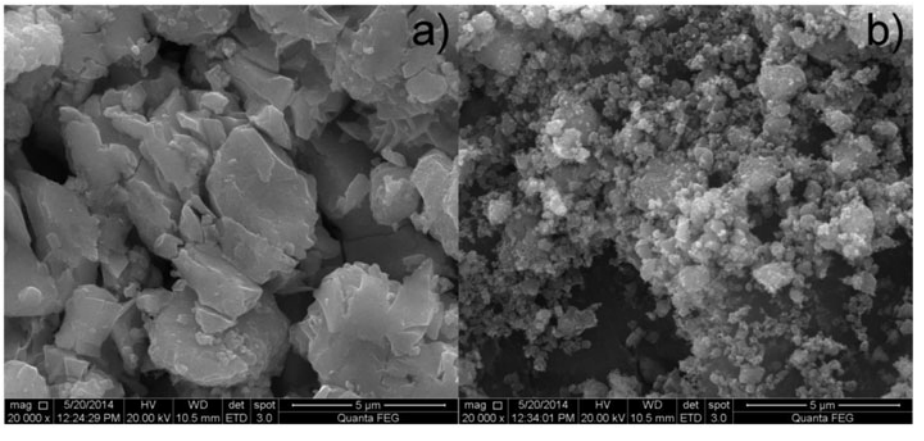

Figure 4. SEM image of (a) $\{Mo_{368}\}$ and (b) $TiO_2@\{Mo_{368}\}$ ethanol dispersion.

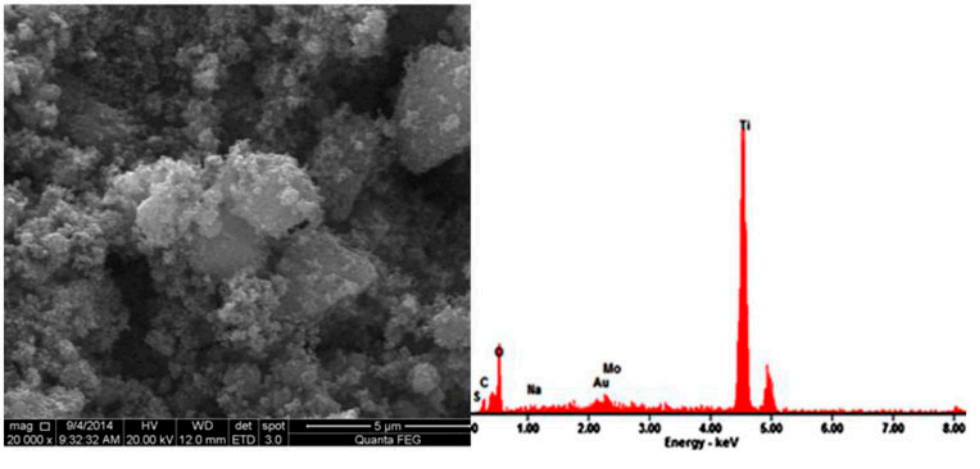

Figure 5. The SEM image and EDX diagram of the composite film of P25-$TiO_2@\{Mo_{368}\}$.

A number of aggregations exist in the composite, which is similar to that of TiO_2@{Mo_{368}}. The EDX analysis demonstrates the existence of Ti, O, Mo, Na, and S, which could confirm that {Mo_{368}} was incorporated into the composite of P25–TiO_2@{Mo_{368}}.

3.3. *Performances of DSSCs*

The performances of DSSCs with two different kinds of photoanodes were detected under simulated AM 1.5 illumination (100 mW cm^{-2}). Seven DSSCs with the P25–TiO_2@{Mo_{368}}-based photoanodes and pure P25-based photoanodes were fabricated, and their photovoltaic parameters are listed in tables 1 and 2, separately. As can be seen, the reproducibility was satisfactory. The set of DSSC with the performance on the intermediate level was selected to represent the average level. The current–voltage (*J–V*) curves show that the performances of DSSCs with P25–TiO_2@{Mo_{368}}-based photoanodes were enhanced compared with that of pure P25-based DSSCs. The inset of figure 6(a) lists their photovoltaic parameters. Through introduction of TiO_2@{Mo_{368}}, the short-circuit current (J_{sc}) was improved from 14.7 to 16.8 mA cm^{-2} with the open-circuit voltage (V_{oc}) increasing from 684 to 711 mV, resulting in enhanced energy conversion efficiency from 6.56 to 7.26%. However, the fill factor (*FF*) of former DSSCs decreased slightly. The improvement of J_{sc} indicated that more electrons were conducted to an external circuit. Figure 6(b) is the dark current curves to determine the electron back-flow processes in DSSCs, which shows that P25-TiO_2@{Mo_{368}}-based DSSCs had smaller dark current than that of pure P25-based DSSCs. This result is consistent with the increased short-circuit photocurrent. Figure 7 shows the photocurrent–time curves when light is regularly switched on and off. It can be concluded that both kinds of DSSCs exhibit the stable photocurrent under continuous

Table 1. Photovoltaic properties of seven parallel DSSCs with the P25-TiO_2@{Mo_{368}}-based photoanodes under simulated AM 1.5 illumination (100 mW cm^{-2}).

	J_{sc} (mA cm^{-2})	V_{oc} (mV)	*FF*	E_{ff} (%)
1	16.43	705	0.632	7.32
2	16.60	722	0.608	7.29
3	16.88	715	0.603	7.28
4	16.80	711	0.608	7.26
5	16.56	703	0.623	7.25
6	16.77	715	0.602	7.22
7	16.86	686	0.622	7.20

Table 2. Photovoltaic properties of seven parallel DSSCs with the pure P25-based photoanodes under simulated AM 1.5 illumination (100 mW cm^{-2}).

	J_{sc} (mA cm^{-2})	V_{oc} (mV)	*FF* (%)	E_{ff} (%)
1	14.12	701	0.658	6.51
2	15.32	705	0.603	6.52
3	14.77	683	0.650	6.55
4	14.69	684	0.653	6.56
5	15.79	666	0.624	6.57
6	15.10	689	0.634	6.60
7	14.86	721	0.617	6.61

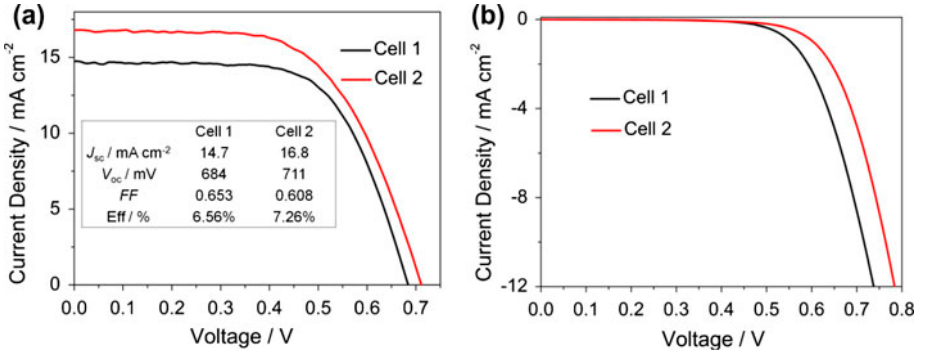

Figure 6. (a) The current–voltage curves of DSSCs with P25-TiO_2@{Mo_{368}}-based photoanodes (red line, cell 2) and pure P25-based ones (dark line, cell 1) under the simulated AM 1.5 illumination; the inset shows their performance parameters; (b) Dark current curves of different DSSCs (see http://dx.doi.org/10.1080/00958972.2014.976211 for color version).

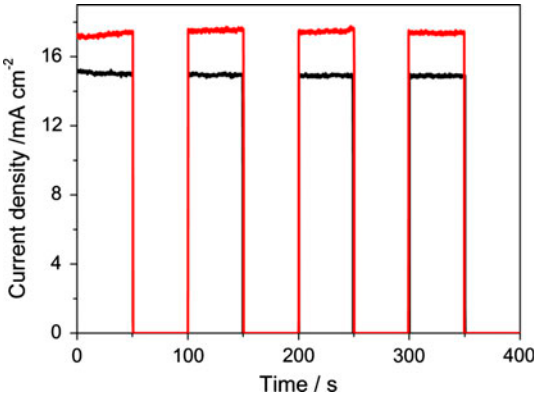

Figure 7. Photocurrent–time curves of two different kinds of DSSCs with 25-TiO_2@{Mo_{368}}-based photoanodes (red line) and pure P25-based ones (dark line) (see http://dx.doi.org/10.1080/00958972.2014.976211 for color version).

illumination, and the higher photocurrent of the former DSSCs is consistent with the result of the *J–V* curve.

Electrochemical impedance spectroscopy (EIS) was performed to understand the electron transport and carrier recombination behavior in the two kinds of DSSCs [26]. Figure 8 gives the typical Nyquist plots of DSSCs, which display two semicircles from high to low frequency corresponding to charge transfer resistance at the interface of the counter electrode and electrolyte (Rpt) and the charge transfer resistance at the TiO_2–dye–electrolyte interface (Rct). As shown in figure 8, the P25-TiO_2@{Mo_{368}}-based cells have larger Rct, which could be beneficial for reducing the carrier recombination for smoother electron transmission. Further, cell 2 exhibits larger series resistance than that of cell 1, and this may be the reason that *FF* of cell 2 decreased. The inset of figure 8 is the Bode phase plots of DSSCs, which give the frequency peaks of the charge transfer processes at different interfaces in DSSCs. The electron lifetime in the photoanode can be calculated from the characteristic low frequency according to equation (1) [27]. The lower frequency in cell 2 corresponds to longer electron lifetime, which contributed to increasing of V_{oc}.

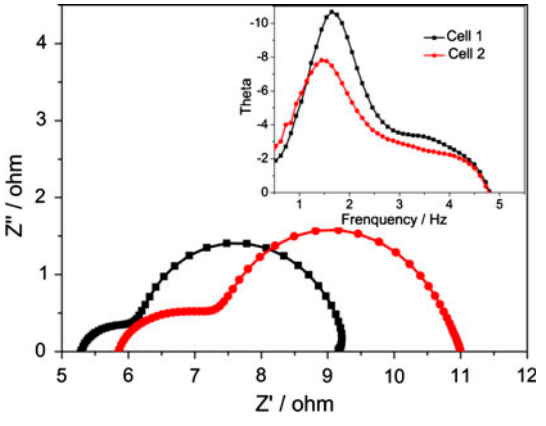

Figure 8. Nyquist plots for the EIS spectra of two different kinds of DSSCs under AM 1.5 solar illumination of 100 mW cm^{-2} at a forward bias of the open-circuit voltage with an ac potential amplitude of 10 mV and a frequency range from 0.1 Hz to 100 kHz; the inset is their bode phase plots.

$$\tau_e = \omega_{\min}{}^{-1} = (2\pi f_{\max})^{-1} \tag{1}$$

Figure 9(a) shows the open-circuit voltage decay (OCVD) curve of DSSCs to monitor the decay of V_{oc} after the illumination has been turned off. It can be seen that V_{oc} of the P25-TiO_2@{Mo_{368}}-based DSSCs decays more slowly than that of pure P25-based cells. This result indicated that the electron back-transfer was effectively inhibited by the introduction of {Mo_{368}}@TiO_2. Further, the electron lifetime could also be obtained by equation (2) [28], which is shown in figure 9(b). The longer electron lifetime in cell 2 indicated that the variation trend is consistent with the result of the EIS analysis.

$$\tau_e = -k_B T / e(dV_{oc}/dt)^{-1} \tag{2}$$

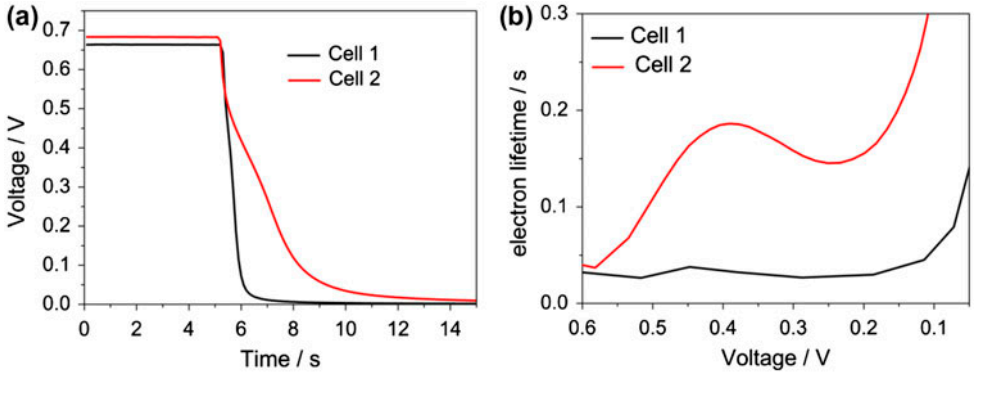

Figure 9. (a) The OCVD curves of the DSSCs with two different kinds of photoanodes; (b) the calculated electron lifetime.

In addition, our DSSCs with the P25-TiO_2@{Mo_{368}}-based photoanodes exhibit much higher *FF* than ones with the P25-TiO_2@SiW_{11}Co-based photoanodes, although the J_{sc} and V_{oc} of our DSSCs are both slightly lower than that of the later ones. As a result, the photoelectric conversion efficiency of our DSSCs with P25-TiO_2@{Mo_{368}}-based photoanodes is higher than that of ones with the P25-TiO_2@SiW_{11}Co-based photoanodes [20]. The detailed information can be seen in table S1 in the Supplementary material.

4. Conclusion

A TiO_2@{Mo_{368}} composite was prepared through a simple sol–gel process. Further, this composite was mixed with P25 then applied as the photoanode of DSSCs, which could enhance the photovoltaic performance of DSSCs through suppressing the dark current and increase the electron lifetime. This work provides a new way for photoelectric functionalization of high-nuclear POMs clusters. Further research on the application of other high-nuclear POMs clusters is currently underway.

Supplementary material

FTIR spectra and TG curve of {Mo_{368}} as well as the comparison of photovoltaic properties of DSSCs with P25-TiO_2@SiW_{11}Co and P25-TiO_2@{Mo_{368}} photoanodes are available online.

Funding

This work was financially supported by the National Natural Science Foundation of China [grant numbers 21131001], [grant number 21201031]; Ph.D station Specialized Research Foundation of Ministry of Education for Universities [grant number 20120043120007]; Science and Technology Development Project Foundation of Jilin Province 500 [grant number 201201072]; the foundation of China Scholarship Council, and the Analysis and Testing Foundation of Northeast Normal University.

References

[1] B. O'Rega, M. Grätzel. *Nature*, **353**, 737 (1991); (b) A. Yella, H.W. Lee, H.N. Tsao, C. Yi, A.K. Chandiran, M.K. Nazeeruddin, E.W.G. Diau, C.Y. Yeh, A.M. Zakeeruddin, M. Grätzel. *Science*, **334**, 629 (2011).
[2] M. Grätzel. *Acc. Chem. Res.*, **42**, 1788 (2009); (b) O.V. Prezhdo, W.R. Duncan, V.V. Prezhdo. *Acc. Chem. Res.*, **41**, 339 (2008).
[3] K. Srikanth, M.D.M. Rahman, H. Tanaka, K.M. Krishna, T. Soga, M.K. Mishra, T. Jimbo, M. Umeno. *Sol. Energy Mater. Sol. Cells.*, **65**, 171 (2001); (b) S. Kobayashi, N. Hamasaki, M. Suzuki, M. Kimura, H. Shirai, K. Hanabusa. *J. Am. Chem. Soc.*, **124**, 6550 (2002).
[4] N. Memarian, I. Concina, A. Braga, S.M. Rozati, A. Vomiero, G. Sberveglieri. *Angew. Chem. Int. Ed.*, **50**, 1 (2011).
[5] D.H. Chen, F.Z. Huang, Y.B. Cheng, R.A. Caruso. *Adv. Mater.*, **21**, 2206 (2009); (b) J.G. Yu, J.J. Fan, L. Zhao. *Electrochim. Acta.*, **55**, 597 (2010).
[6] S.Y. Huang, G. Schlichthörl, A.J. Nozik, M. Grätzel, A.J. Frank. *J. Phys. Chem. B.*, **101**, 2576 (1997).
[7] J.Y. Zhang, Z.Y. Zhao, X.Y. Wang, T. Yu, J. Guan, Z.T. Yu, Z.S. Li, Z.G. Zou. *J. Phys. Chem. C.*, **114**, 18396 (2010); (b) X. Zhang, F. Liu, Q.L. Huang, G. Zhou, Z.S. Wang. *J. Phys. Chem. C.*, **115**, 12665 (2011).
[8] L. Sun, L. Gao, Y. Liu. *Appl. Phys. Lett.*, **96**, 113 (2010).

[9] H. Fu, C. Qin, Y. Lu, Z.M. Zhang, Y.G. Li, Z.M. Su, W.L. Li, E.B. Wang. *Angew. Chem. Int. Ed.*, **51**, 7985 (2012); (b) P.C. Yin, P.F. Wu, Z.C. Xiao, D. Li, E. Bitterlich, J. Zhang, P. Cheng, D.V. Vezenov, T.B. Liu, Y.G. Wei. *Angew. Chem. Int. Ed.*, **50**, 2521 (2011); (c) N.V. Izarova, M.T. Pope, U. Kortz. *Angew. Chem. Int. Ed.*, **51**, 9492 (2012); (d) Z.H. Kang, E.B. Wang, L. Gao, S.Y. Lian, M. Jiang, C.W. Hu, L. Xu. *J. Am. Chem. Soc.*, **125**, 13652 (2003).
[10] A. Hiskia, A. Mylonas, E. Papaconstantinou. *Chem. Soc. Rev.*, **30**, 62 (2001).
[11] Z.X. Sun, L. Xu, W.H. Guo, B.B. Xu, S.P. Liu, F.Y. Li. *J. Phys. Chem. C.*, **114**, 5211 (2010); (b) S. Anandan, S. Pitchumani, B. Muthuraaman, P. Maruthamuthu. *Sol. Energy Mater. Sol. Cells.*, **90**, 1715 (2006); (c) H. Park, W. Choi. *J. Phys. Chem. B*, **107**, 3885 (2003); (d) J.S. Li, X.J. Sang, W.L. Chen, C. Qin, S.M. Wang, Z.M. Su, E.B. Wang. *Eur. J. Inorg. Chem.*, **2013**, 1951 (2013); (e) X.J. Sang, J.S. Li, W.L. Chen, E.B. Wang. *Mater. Lett.*, **87**, 39 (2012); (f) J.S. Li, X.J. Sang, W.L. Chen, L.C. Zhang, Z.M. Su, C. Qin, E.B. Wang. *Inorg. Chem. Commun.*, **38**, 78 (2013).
[12] S.M. Wang, L. Liu, W.L. Chen, E.B. Wang, Z.M. Su. *Dalton Trans.*, **42**, 2691 (2013).
[13] A. Müller, F. Peters, M.T. Pope, D. Gatteschi. *Chem. Rev.*, **98**, 239 (1998).
[14] U. Kortz, M.G. Savelieff, B.S. Bassil, M.H. Dickman. *Angew. Chem. Int. Ed.*, **40**, 3384 (2001).
[15] T.B. Liu, M.L.K. Langston, D. Li, J.M. Pigga, C. Pichon, A.M. Todea, A. Muller. *Science*, **331**, 1590 (2011).
[16] G. Jin, S.M. Wang, W.L. Chen, C. Qin, Z.M. Su, E.B. Wang. *J. Mater. Chem. A.*, **1**, 6727 (2013).
[17] A. Müller, P. Kögerler. *Chem. Rev.*, **182**, 3 (1999); (b) A. Müller, Q.N. Shah, H. Bögge, M. Schmidtmann. *Nature*, **397**, 48 (1999).
[18] A. Müller, E. Beckmann, H. Bögge, M. Schmidtmann, A. Dress. *Angew. Chem. Int. Ed.*, **41**, 7 (2002).
[19] A. Müller, B. Botar, S.K. Das, H. Bögge, M. Schmidtmann, A. Merca. *Polyhedron*, **23**, 2381 (2004).
[20] L. Li, Y.L. Yang, R.Q. Fan, X. Wang, Q.M. Zhang, L.Y. Zhang, B. Yang, W.W. Cao. *Dalton Trans.*, **43**, 1577 (2013).
[21] S. Ito, P. Chen, P. Comte, M.K. Nazeeruddin, P. Liska, P. Péchy, M. Grätzel. *Prog. Photovolt: Res. Appl.*, **15**, 603 (2007).
[22] X. López, C. Bo, J.M. Poblet. *J. Am. Chem. Soc.*, **124**, 12574 (2002).
[23] T. Tachikawa, S. Tojo, M. Fujitsuka, T. Majima. *Chem. Eur. J.*, **12**, 3124 (2006).
[24] J.L.G. Fierro, L.A. Arrua, J.M.L. Lopez Nieto, G. Kremenic. *Appl. Catal.*, **37**, 323 (1988); (c) A.A. Galuska, J.C. Uht, N. Marquez. *J. Vac. Sci. Technol., A*, **6**, 110 (1988).
[25] T.A. Patterson, J.C. Carver, D.E. Leyden. *J. Phys. Chem.*, **80**, 1700 (1976); (b) H.M. Wu, S.A. Chen. *Synth. Met.*, **26**, 225 (1988).
[26] Q. Wang, J.E. Moser, M. Grätzel. *J. Phys. Chem. B.*, **109**, 14945 (2005).
[27] Y.Z. Zheng, X. Tao, L.X. Wang, H. Xu, Q. Hou, W.L. Zhou, J.F. Chen. *Chem. Mater.*, **22**, 928 (2010).
[28] J. Bisquert, A. Zaban, M. Greenshtein, I.M. Sero. *J. Am. Chem. Soc.*, **126**, 13550 (2004).